

# $\mu$ -PhotoZ: Photometric Redshifts by Inverting the Tolman Surface Brightness Test

Michael J. Kurtz, Margaret J. Geller, Daniel G. Fabricant, William F. Wyatt

*Harvard-Smithsonian Center for Astrophysics, Cambridge, MA 02138*

and

Ian P. Dell'Antonio

*Brown University, Department of Physics and Astronomy*

*email: kurtz@cfa.harvard.edu*

## ABSTRACT

Surface brightness is a fundamental observational parameter of galaxies. We show, for the first time in detail, how it can be used to obtain photometric redshifts for galaxies, the  $\mu$ -PhotoZ method.

We demonstrate that the Tolman surface brightness relation,  $\mu \propto (1+z)^{-4}$ , is a powerful tool for determining galaxy redshifts from photometric data.

We develop a model using  $\mu$  and a color percentile (ranking) measure to demonstrate the  $\mu$ -PhotoZ method. We apply our method to a set of galaxies from the SHELS survey, and demonstrate that the photometric redshift accuracy achieved using the surface brightness method alone is comparable with the best color-based methods.

We show that the  $\mu$ -PhotoZ method is very effective in determining the redshift for red galaxies using only two photometric bands. We discuss the properties of the small, skewed, non-gaussian component of the error distribution.

We calibrate  $\mu_r, (r-i)$  from the SDSS to redshift, and tabulate the result, providing a simple, but accurate look up table to estimate the redshift of distant red galaxies.

*Subject headings:* methods: data analysis  
techniques: photometric redshifts  
techniques: surface brightness analysis

## 1. Introduction

Tolman (1930) and Hubble & Tolman (1935) first showed that in an expanding universe the surface brightness of a galaxy is a strong function of the redshift,  $SB \propto (1+z)^{-4}$ , or  $\mu = \mu_0 + 10\log(1+z)$ . Hubble & Tolman (1935) suggested that this effect could be used as a distance indicator and as a test of various cosmological scenarios (the Tolman test).

Baum (1957) was the first to show that the shifting of spectral features as a function of redshift (in particular the 4000Å break) causes color changes which can be calibrated to estimate a redshift. Interestingly the discussion with Hoyle following Baum (1962) demonstrates an understanding that this effect might be combined with or be complementary to the surface brightness effect for redshift estimation. At the time of the discussion, the steady state hypothesis was still quite viable, and thus the exact nature of the surface brightness effect was not known. More recently Sandage & Lubin (2001) and Pahre et al. (1996) measured the effect; various systematics, including galaxy luminosity evolution, prevent these measures from being definitive, but the true relation is very close to  $(1+z)^{-4}$ .

Typically, photometric redshifts are derived from color differences as a function of total magnitude. Some techniques fit model spectra (e.g. Baum 1957; Budavári et al. 2001; Bolzonella et al. 2000), others directly calibrate the dataset (e.g. Firth et al. 2003; Kodama et al. 1999; Feldmann et al. 2006), and still others combine these two methods into a hybrid (e.g. Padmanabhan et al. 2005, P05). Several proponents of the neural network method remark that surface brightness related measures could be added to their ingest parameters (e.g. Margoniner et al. 2005; Suchkov et al. 2005). By including the Petrosian 50% and 90% flux radii Wadadekar (2005) found a 15% improvement in the mean redshift error.

Here we demonstrate that surface brightness provides a highly effective redshift estimator for the reddest galaxies in each surface brightness interval, yielding very accurate photometric redshifts from either  $r$  and  $i$ , or  $r$  and  $z$  band observations. We indicate how other color combinations might be used. We present the  $\mu_r, (r-i)$  calibration to redshift for red galaxies in the SDSS. One powerful advantage of this method is that only two bands are required for its application.

We present the data in section 2 and in section 3 we introduce the  $\mu$ -PhotoZ technique, and discuss its physical basis and limitations. We briefly indicate the extension of our technique to other bandpasses in section 4. The technique is applied in section 5 and we discuss the nature of the error distribution in detail. In section 6 we apply our method to the SDSS.

## 2. Data

We combine data from three large surveys to create a set of measures suitable for demonstration of the  $\mu$ Photo- $z$  technique; (i) a magnitude limited galaxy catalog from the Deep Lens Survey (Wittman et al. 2006, DLS), (ii) redshifts and spectral types from the Smithsonian Hectospec Lensing Survey (Geller et al. 2005, SHELS), and (iii) photometry and spectroscopy from the fourth and fifth data releases of the Sloan Digital Sky Survey (Adelman-McCarthy et al. 2006, SDSS).

### 2.1. DLS

SHELS used the DLS deep R band photometry from the  $2^\circ \times 2^\circ$  field F2 (9:20+30:00) to select galaxies for redshift measurements with the Hectospec (Fabricant et al. 2005). We used the difference between magnitudes within the  $1.5''$  and  $5''$  apertures and the FWHM to a gaussian fit as star/galaxy classifiers. It is possible to derive photometric redshifts based on *colors* from the deep multicolor DLS data (Margoniner, et al, in preparation).

The extended (scattering) halos around bright stars significantly contaminate the brightness measures of faint galaxies. We have excluded all objects within a magnitude determined radius of every bright star; about 5% of the total area of the survey is thus removed from further consideration.

### 2.2. SDSS

From the SDSS we use the Petrosian  $r$  magnitudes (for a discussion of the advantages of Petrosian magnitudes for cosmological investigations see Strauss et al. 2002), the star/galaxy classifications, and the colors derived from the fiber magnitudes. From the Petrosian half light radii (in the  $r$  band) we calculate the central surface brightness  $\mu_r$ , the average surface brightness (in  $r$  mag per arcsec squared inside the half light radius);

$$\mu_r \equiv \text{petroMag}_r + 2.5(0.798 + 2\log(\text{petroRad50}_r))$$

All measures are extinction corrected.

In section 6 we calibrate the  $\mu_r, (r - i)$  plane to redshift for the SDSS, using  $\mu_r, (r - i)$  and redshift.

### 2.3. SHELS

The SHELS will be a magnitude limited redshift survey when complete. We use the data set as of 1 January 2006. Our data set is 90% complete to  $R < 19.7$  and is 50% differentially complete at  $R = 20.3$ , using DLS total magnitudes.

From the full SHELS dataset we eliminated all objects in the vicinity of bright stars (about 5%); we discard any object where the DLS position differs from the SDSS position by more than  $1''$ ; we use only galaxies with spectra with secure redshifts. The final sample contains 8529 redshifts of the estimated final 12,000.

### 2.4. The Combination

The key dataset required for the  $\mu$ -PhotoZ technique is a photometrically complete sample of galaxies with accurate central surface brightnesses and at least one color. For this paper we primarily use  $\mu_r$  and the  $r - i$  color from the SDSS-DR4. In addition we derive a set of pseudo-magnitudes:  $\mu_g = \mu_r + (g - r)$ ;  $\mu_i = \mu_r - (r - i)$ ;  $\mu_z = \mu_r - (r - z)$ , these are estimates of the surface brightness inside the half-light radius defined by the  $r$  band.

## 3. Technique

Surface brightness, which, in an expanding universe changes as  $(1 + z)^{-4}$  (Tolman 1930), is a much more sensitive indicator of redshift than apparent magnitude. Unlike apparent magnitude, surface brightness has no dependence on the details of the cosmology (e.g. Sandage 1975).

The change in the observed surface brightness of a galaxy is the product of the change in brightness due to the use of a static (non-redshifted) bandpass (the K correction Hubble 1936) and the cosmological dimming. Figure 1 shows these effects in terms of the measured dimming in magnitudes as a function of the redshift of the object. The line on the left is the K correction for  $r$  band measurements of brightest cluster galaxies calculated by Annis (2001) using the Pegase code (Le Borgne & Rocca-Volmerange 2002). The thin line in the middle is simply  $10\log(1 + z)$ , and the thick line on the right is the product of the two effects.

When the galaxies in the catalog are binned according to  $\mu_r$ , and then sorted by color, the reddest 10-20% of the galaxies in each  $\mu_r$  bin show a very strong correlation between  $\mu_r$  and redshift.

Figure 2 explains this correlation. The y axis is simply the  $r - i$  color. The x axis represents the surface brightness dimming expected from the sum of the appropriate K correction and the  $10\log(1 + z)$  effect. The lines on the plot represent the  $r - i$  color of galaxies computed by subtracting the Annis (2001) K correction model in the  $i$  band from the model in the  $r$  band. On the left the two lines represent the BCG galaxy model (black) and that model shifted 0.5 mag (dashed green) to approximate the extent of the scatter. On the right, figure 2 shows the model for an Sa galaxy (black), we have shifted the zero point of the Sa relation by 0.46 mag to account for the difference in  $\mu_r$  between a  $r^{\frac{1}{4}}$  law galaxy and an exponential disk with the same scale length and total magnitude (Strauss et al. 2002). Redshift increases along the lines.

The small red circles show the observed  $r - i$  color and  $\mu_r - const.$  for those galaxies in the reddest 10% in each  $\mu_r$  bin which have a measured redshift, and the small blue triangles show the 20-30% reddest objects in each bin. As expected, the redder objects lie mainly between the two BCG lines, and the bluer objects approximately follow the SA line, validating our use of these models.

A successful technique which calibrates red galaxies to redshift must be free of contamination by higher redshift blue objects at the same color. Figure 2 shows that surface brightness eliminates much of the possible confusion. There are, however, regions in figure 2 where lines cross, or come close to each other, indicating degeneracies.

There are three sets of large geometric figures on the plot: the left (bottom) two (circles and triangles) show regions where there could be confusion between BCG galaxies and Sa galaxies, indicating possible problems for the technique; the right (top) square(s), which overlap perfectly, show where BCG galaxies no longer become redder in  $r - i$  with increasing redshift, indicating a limit to the  $\mu$ -PhotoZ technique.

The circles on the bottom left show where the BCG galaxy is at  $z=0.15$  and the SA galaxy is at  $z=0.24$ . Clearly if a calibration of red objects to redshift as a function of  $\mu_r$  succeeds at this redshift it is not because it separates early type galaxies from SA galaxies.

The pair of triangles are at  $z=0.4$  for the BCG and  $z=0.5$  for the SA. They are close enough to present a potential problem. We note that P05 found increased scatter in their calibration of photometric redshifts for LRG galaxies at  $z=0.4$ , but attributed it to other causes. Notice that it is the (approximately) 0.45 magnitude difference between the BCG and Sa central surface brightnesses at a fixed magnitude which separates the types in the color-magnitude diagram in figure 2; previous methods, such as P05, use total magnitudes and additional colors. Using surface brightness breaks this degeneracy for galaxies with different surface brightness profiles, without requiring additional colors be observed.

The top square(s), at  $z=0.65$  for the unshifted BCG locus and  $z=0.765$  for the shifted locus clearly shows a region where the  $10\log(1+z)$  dimming is insufficient to remove degeneracies.

To summarize the technique: using a complete photometric catalog (e.g. SDSS) we (1) bin galaxies according to a measure of central surface brightness, such as  $\mu_r$ , then (2) in each bin, we sort the galaxies by a measure of color, such as  $r-i$ . Next (3) we assign a percentile rank to each galaxy based on its color, within each surface brightness bin.

As an example, in the F2 field there are 2506 galaxies with  $\mu_r$  between 22.6 and 22.8; a galaxy at  $\mu_r = 22.79$  and with  $r-i = 0.965$  is redder than 96.2% of the galaxies in its bin, and receives a color percentile of 96.2. Likewise a galaxy with  $\mu_r = 22.38$  and with  $r-i = 0.769$  is redder than 96.2% of the 1551 galaxies in the 22.2-22.4  $\mu_r$  magnitude bin. Note that both galaxies have a color rank score of 96.2 but have substantially different actual  $r-i$  colors.

These color rank percentile (CRP) scores are strongly correlated with galaxy type; in the next section we demonstrate their usefulness in permitting a calibration of central surface brightness to redshift for the redder objects.

### 3.1. Results

Figure 3 shows the result of plotting  $\mu_r$  vs. redshift for galaxies within ten decile bins in CRP scores. We compute ranks using the  $r-i$  color. The red dots are for spectra where the measured O[II] 3727Å equivalent width is  $> -2\text{Å}$  and the blue circles have clearly measurable emission, ( $EQW_{3727} < -2\text{Å}$ ). The solid lines are the Annis (2001)  $r$  BCG K correction times  $10\log(1+z)$  shifted to match  $\mu_r = 20.0$  mag per square arcsec at redshift zero.

There are several things to notice in figure 3. First the galaxies in the reddest deciles in CRP follow the prediction of the Annis (2001) BCG K correction times  $10\log(1+z)$  very closely. The next decile is slightly offset from the reddest. Clearly the calibration of  $\mu_r$  to redshift for galaxies in these CRP deciles is straightforward.

Next we notice that the bluest objects show essentially no correlation between  $\mu_r$  and redshift, the available  $\mu_r - z$  space in the bluest decile in CRP is nearly uniformly filled. Clearly  $\mu_r$  cannot be calibrated to redshift for the bluest objects, which have their surface brightnesses altered by star formation.

Figure 4 shows the result of fitting  $\mu_r$  to redshift by finding the redshift,  $z$ , where for

the  $i^{\text{th}}$  galaxy,

$$\mu_r(i) = K_i(z) + 10\log(1+z) + 19.45 + 3.3(1 - CRP(i))$$

(the model). The factor containing CRP accounts for the change in  $\mu_r$  with color, variously quantified as the color-magnitude relation for elliptical galaxies (e.g. Baum 1959; Visvanathan & Sandage 1977; Chang et al. 2006; Cool et al. 2006; Eisenhardt et al. 2006) or as the fundamental plane (e.g. Djorgovski & Davis 1987; Bernardi et al. 2003).

The standard deviation for the entire sample of the reddest 10% in figure 4 is  $\sigma(\Delta z/1+z) = 0.046$  and is  $\sigma = 0.056$  for the reddest 10–20%. This result is comparable with the best current photometric redshifts for the LRG galaxies. P05 obtain  $\sigma = 0.035$  using  $g$  photometry as well as  $r$  and  $i$  (see section 5).

#### 4. Using other colors and magnitudes

As figure 2 shows, the  $\mu$ -PhotoZ technique becomes degenerate when the 4000Å break enters the bandpass of the reddest band ( $i$  in figure 2). To acquire  $\mu$ -PhotoZs for higher redshift objects observations in a redder passband ( $z$ , J, H, etc) would extend the technique to higher redshifts. Neither the SHELS spectroscopy nor the SDSS photometry go deep enough to test the technique for redshifts greater than 0.65 using  $z$  band photometry.

Obviously other bandpasses may also be used. There are three different choices to make: (1) the bandpass to use to sort the colors, (2) the color to use, and (3) the bandpass to fit. Here we have used  $\mu_r$ ,  $(r-i)$ , and  $\mu_r$ , but other choices are informative. Figure 5 shows galaxies in the the reddest 10% as determined using  $\mu_r$  and  $(r-i)$  versus  $\mu_z, \mu_i, \mu_r, \mu_g$ , along with the sum of  $10\log(1+z)$  and the appropriate Annis (2001) BCG K correction for each color. Redshift estimates using  $z$  and  $g$  band data have larger errors than estimates using  $r$  and  $i$ , in the manner expected from the larger published errors in the SDSS magnitudes for these bands.

One might also ask whether the technique of using color ranks might also work if one uses total magnitude rather than central surface brightness. Figure 6 shows (left side) galaxies in the the reddest 10% in  $(r-i)$  measured at fixed Petrosian  $r$  magnitude versus Petrosian  $r$ , and (right side) galaxies in the reddest 10% in  $(r-i)$  measured at fixed  $\mu_r$  versus  $\mu_r$ ; each grouping has two lines to guide the eye. These lines are the product of the K correction and the surface brightness dimming. The separation is an arbitrary one magnitude.

Clearly the scatter in the Petrosian magnitude measures in figure 6 is larger than in the  $\mu_r$  measures. Figure 2 explains this behavior. Recall that we shifted the line represent-

ing the K correction and surface brightness dimming by 0.46 magnitudes to account for a 0.46 difference in the mean central surface brightness at fixed total magnitude for the two galaxy types (BCG and Sa), and this procedure matched the data. Shifting the Sa line 0.46 magnitudes brightward would place it much closer to the BCG line, and would thus produce substantially more degeneracy in the color rank approach.

## 5. Calibrating the Relation Directly

In section 3.1 we demonstrated that we can predict the redshift of a red galaxy accurately from a measure of its central surface brightness and a single color ( $r - i$ ). We fitted models based on estimates of the K-correction, the color-magnitude relation for elliptical galaxies, and the  $(1 + z)^{-4}$  cosmological dimming to measures of color and surface brightness.

We may not have used the best model parameters in making these fits, and we can also suspect that our measure of central surface brightness,  $\mu_r$  could have measurement systematics which correlate with redshift. Although these models are useful in understanding the physical basis for the technique, they are not actually required to implement it.

Rather than attempt to optimize the models and measures, we choose to calibrate the data directly. To each galaxy we assign the median redshift of its neighbors in  $(\mu_r, \text{CRP})$  space, excluding the galaxy itself, in jack-knife fashion.

Figure 7 shows the distribution of absolute values of the residuals (in terms of  $\Delta z / (1 + z)$ ); the thick black lines represent the residuals of the actual data (top represents galaxies in the 80-90 color percentile range, bottom represents those in the 90-100 color percentile range), sorted from smallest to largest. The dotted lines show the distributions expected for normal error distributions with  $\sigma$ s of (bottom to top) 0.02, 0.03, 0.04, and 0.05. The tails of the error distribution are clearly not gaussian, but the errors are small. Eighty percent of all objects in the reddest decile have errors smaller than would be expected for a normal error distribution with a  $\sigma$  of 0.03.

About 40% of the high residual objects are low redshift galaxies that are anomalously blue in  $g - r$ . These objects could easily be removed in a three band survey. For example, the thin solid line in figure 7 shows the error distribution for the same sample as the bottom solid line, but with all objects with  $g - r < 1.4$  removed. The tails of the distribution are substantially reduced.

Figure 8 shows the distribution of residuals for the reddest 20% (excluding  $g - r < 1.4$ )  $\frac{(z_{measured} - z_{estimated})}{1+z}$  with a  $\sigma = 0.025$  gaussian overplotted (1272 objects with redshifts). These

results show that  $\mu$ -PhotoZ redshifts are as accurate as the best photometric redshifts, (e.g. P05). The  $1\sigma$  RMS for the data in figure 8 is 0.030, P05 obtain 0.035. The  $(\mu_r, CRP) - z$  calibration works well for all galaxies with  $(g - r) > 1.4$ . The  $1\sigma$  RMS for all these 2399 galaxies with redshifts is 0.037.

Figure 7 clearly indicates that the  $\mu$ -PhotoZ method provides estimated redshifts from a single color, such as  $r - i$ , albeit with increased errors and a non-gaussian error component. Figure 9 shows the error distribution  $\frac{\Delta z}{1+z}$  for the 330 galaxies from SHELS which are in the reddest 20% and which have  $g - r < 1.4$ ; two gaussians, with  $\sigma = 0.03; 0.06$  are also plotted.

The error distribution in figure 9 for  $\frac{\Delta z}{1+z}$  can be reasonably fit by a gaussian with  $\sigma = 0.06$  and a non-gaussian tail, where the actual redshifts are always smaller than the estimated ones. A description of the tail, consistent with the current data, is that the objects are randomly located in the galaxy distribution in the foreground of its apparent (as estimated by  $\mu$ -PhotoZ) position,  $z_{est}$ .

For the entire sample of the 20% reddest galaxies, without removing any objects using a third band, the error distribution for  $z_{est}$ :

$$Err_{z_{est}} = 0.79G(.03) + 0.16G(.06) + 0.05R(N(z)); (z < z_{est})$$

where  $G(x)$  is a gaussian with  $\sigma = x$ ;  $R(x)$  is a random deviate from the distribution  $x$ , and  $N(z)$  is the redshift distribution of the “foreground” galaxies.

## 6. Calibration the SDSS $\mu_r, (r - i)$ to redshift relation for red galaxies

The color percentile measure at any fixed surface brightness corresponds directly to an actual color. To provide a calibration for the SDSS we simply find the median redshift for galaxies in small cells in  $\mu_r, (r - i)$ .

We use the SDSS-DR5 and find the 62,259 galaxies with  $20.35 < \mu_r < 23.25$  and  $0.475 < (r - i) < 1.225$  and with  $(g - r) > 1.4$  which have measured redshifts. 59,905 redshifts come from the SDSS, essentially the LRG sample (Eisenstein et al. 2001), and 2,345 redshifts come from SHELS, mainly for fainter galaxies. There are 64 objects in common. The redshifts agree, save for one case where SDSS found a star and SHELS found a galaxy.

To estimate the error in the redshift estimator we take, for each cell, the galaxies in the cell and assign to them the median redshift for that cell. We then rank the absolute value of the residuals for the galaxies in that cell. The median residual, for a gaussian distribution would be  $0.67\sigma$ , the 68<sup>th</sup> percentile would be  $1\sigma$  and the 95<sup>th</sup> percentile would be  $2\sigma$ . We

only estimate the  $1\sigma$  point if there are at least 15 galaxies in a bin, and the  $2\sigma$  point if there are more than 30.

Table 1 displays the results for bins with small and well determined residuals in a convenient form. The typeface indicates the error. Use of this table allows quick and reasonably accurate estimation of redshifts for red galaxies in the SDSS photometric database reaching to a redshift of approximately 0.5.

## 7. Discussion

Surface brightness is a fundamental observational parameter of galaxies; it is directly related to redshift through the classical Tolman effect. We believe this investigation is the first to show in detail that surface brightness may be used directly as a measure of redshift, the  $\mu$ -PhotoZ method.

We demonstrate the value of surface brightness measures in determining photometric redshifts using three different techniques. First, we use a model which emphasizes the physical and measurement aspects of the problem. Next, we demonstrate that by assigning a galaxy the median redshift of its neighbors in surface brightness, color percentile space we can achieve photometric redshift errors comparable with the best current photometric redshift methods. Finally by taking the median redshift in small bins in surface brightness–color space we develop a redshift estimator with errors comparable with the best techniques.

Although we have concentrated on the use of  $\mu_r$  and  $(r - i)$  for nearby red galaxies the techniques discussed here have much greater generality; the  $(1 + z)^{-4}$  cosmological dimming effects all galaxies at all redshifts. Adding surface brightness directly into model fitting and hybrid methods seems a very profitable avenue to explore.

Obviously the technique could be extended to greater redshift for red galaxies by using the  $z$  band. Deep, large area lensing surveys, including the DLS, often have deep  $z$  photometry, and thus can obtain photometric redshifts out to a redshift of about 1, using the methods shown here. These deeper surveys will also be able to eliminate some of the non-gaussian error apparent in the SDSS photometry. Much of this error results from SDSS failure to separate close pairs of faint objects (star + galaxy or galaxy + galaxy). With much deeper imaging and better seeing these effects should be less troublesome.

As the discussion in section 5 makes clear, most of the benefit from applying the  $\mu$ -PhotoZ technique is achieved by using just two photometric bands. This powerful aspect of the technique has obvious implications for the design of large area weak lensing surveys. It is

exactly the high central surface brightness red galaxies analyzed in section 5 which have the highest redshift at fixed central surface brightness (figure 3), and central surface brightness is the limiting factor in determining the shape parameters for the sources. Our technique makes feasible substantially larger area weak lensing surveys than would be possible were it necessary to observe through several filters.

## 8. Acknowledgments

We thank Scott Kenyon for discussions, and we thank Tony Tyson, David Wittman and Vera Margoniner for their collaboration in obtaining the initial galaxy catalog. We thank Ken Rines and Warren Brown for a careful reading of the manuscript. This research was supported in part by the Smithsonian Institution.

*Facilities:* MMT(Hectospec), SDSS, KPNO(Mayall).

## REFERENCES

- Adelman-McCarthy, J. K., et al. 2006, ApJS, 162, 38
- Annis, J. 2001, <http://home.fnal.gov/~annis/astrophys/kcorr/kcorr.html>
- Baum, W. A. 1957, AJ, 62, 6
- Baum, W. A. 1959, PASP, 71, 106
- Baum, W. A. 1962, IAU Symp. 15: Problems of Extra-Galactic Research, 15, 390
- Bernardi, M., et al. 2003, AJ, 125, 1866
- Bolzonella, M., Miralles, J.-M., & Pelló, R. 2000, A&A, 363, 476
- Budavári, T., et al. 2001, AJ, 122, 1163
- Chang, R., Shen, S., Hou, J., Shu, C., & Shao, Z. 2006, MNRAS, 372, 199
- Cool, R. J., Eisenstein, D. J., Johnston, D., Scranton, R., Brinkmann, J., Schneider, D. P., & Zehavi, I. 2006, AJ, 131, 736
- Csabai, I., et al. 2003, AJ, 125, 580
- Djorgovski, S., & Davis, M. 1987, ApJ, 313, 59

- Eisenhardt, P. R., De Propriis, R., Gonzalez, A., Stanford, S. A., Dickinson, M. E., & Wang, M. C. 2006, ArXiv Astrophysics e-prints, arXiv:astro-ph/0611873
- Eisenstein, D. J., et al. 2001, AJ, 122, 2267
- Fabricant, D., et al. 2005, PASP, 117, 1411
- Feldmann, R., et al. 2006, MNRAS, 372, 565
- Firth, A. E., Lahav, O., & Somerville, R. S. 2003, MNRAS, 339, 1195
- Geller, M. J., Dell’Antonio, I. P., Kurtz, M. J., Ramella, M., Fabricant, D. G., Caldwell, N., Tyson, J. A., & Wittman, D. 2005, ApJ, 635, L125
- Hubble, E. 1936, ApJ, 84, 517
- Hubble, E., & Tolman, R. C. 1935, ApJ, 82, 302
- Kodama, T., Bell, E. F., & Bower, R. G. 1999, MNRAS, 302, 152
- Le Borgne, D., & Rocca-Volmerange, B. 2002, A&A, 386, 446
- Margoniner, V. E., Connolly, A., & Tyson, J. A. 2005, Bulletin of the American Astronomical Society, 37, 1206
- Padmanabhan, N., et al. 2005, MNRAS, 359, 237
- Pahre, M. A., Djorgovski, S. G., & de Carvalho, R. R. 1996, ApJ, 456, L79
- Sandage, A. 1975, in Galaxies and the Universe. Eds. Allan Sandage, Mary Sandage, and Jerome Kristian, with an index prepared by Gustav A. Tammann. Published by the University of Chicago Press (Stars and Stellar Systems. Volume 9), Chicago, IL USA., 1975, p.761
- Sandage, A., & Lubin, L. M. 2001, AJ, 121, 2271
- Strauss, M. A., et al. 2002, AJ, 124, 1810
- Suchkov, A. A., Hanisch, R. J., & Margon, B. 2005, AJ, 130, 2439
- Tolman, R. C. 1930, Proceedings of the National Academy of Science, 16, 511
- Visvanathan, N., & Sandage, A. 1977, ApJ, 216, 214
- Wadadekar, Y. 2005, PASP, 117, 79

Wittman, D., Dell’Antonio, I. P., Hughes, J. P., Margoniner, V. E., Tyson, J. A., Cohen, J. G., & Norman, D. 2006, *ApJ*, 643, 128

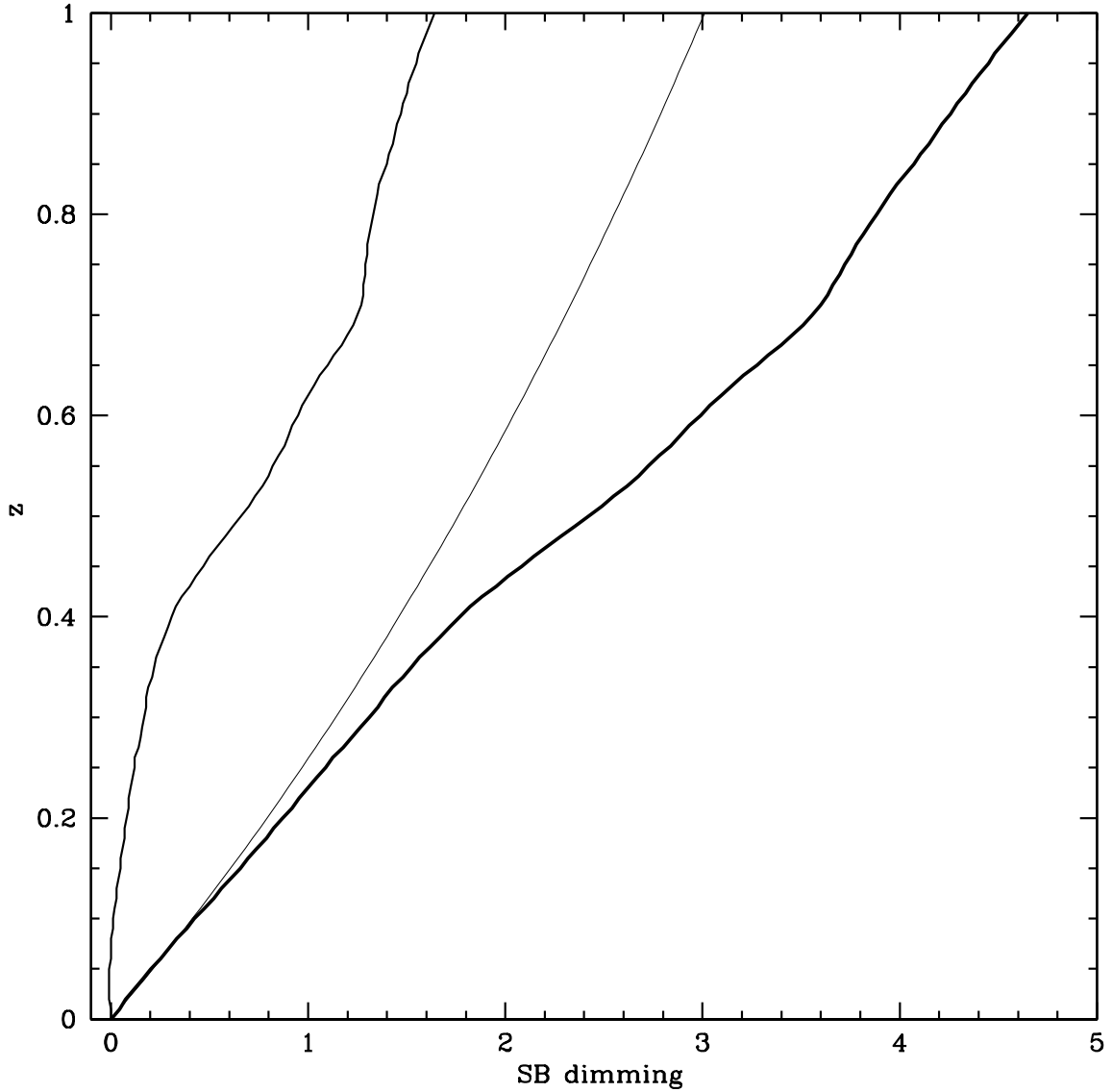


Fig. 1.— Combining the K correction with surface brightness dimming, in magnitudes, as a function of redshift. The Annis (2001)  $r$  band BCG K correction is on the left, the thin line in the center is  $10\log(1+z)$ , and the thick line on the right is the sum of the two effects.

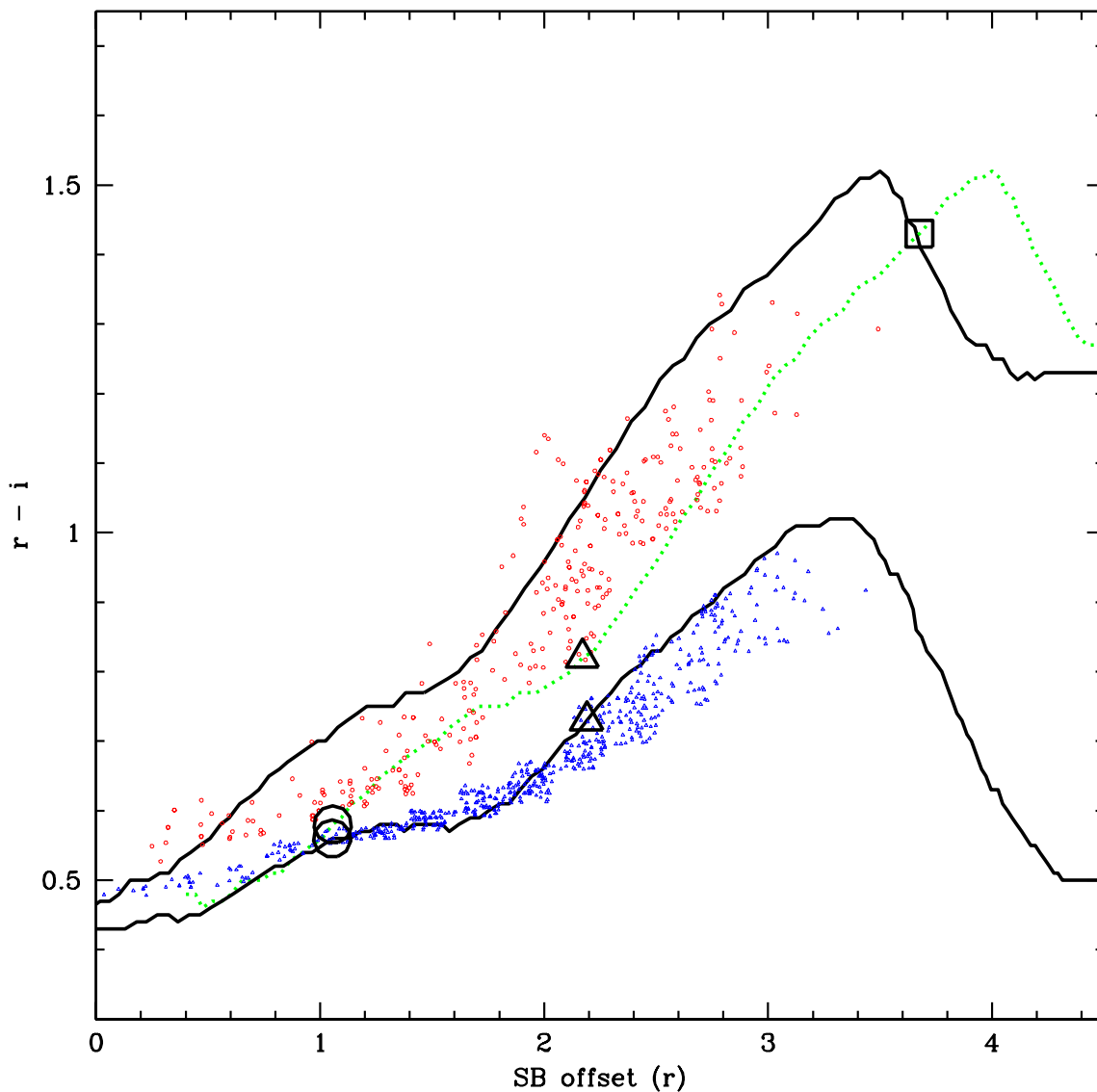


Fig. 2.— Color vs. surface brightness dimming for different galaxy types. The x axis is the Annis (2001)  $r$  band K correction plus  $(1+z)^{-4}$  and the y axis is the difference between the the K corrected  $r$  band and  $i$  band. Redshift increases along the lines. The left most lines represent the BCG K correction, with the right (green on-line) one shifted by 0.5 mag with respect to the other. The right most line is the Sa K correction. The points represent the (red) reddest 10% and (blue) the reddest 20–30% of galaxies in the SHELS sample. The large geometric figures point to interesting regions described in the text.

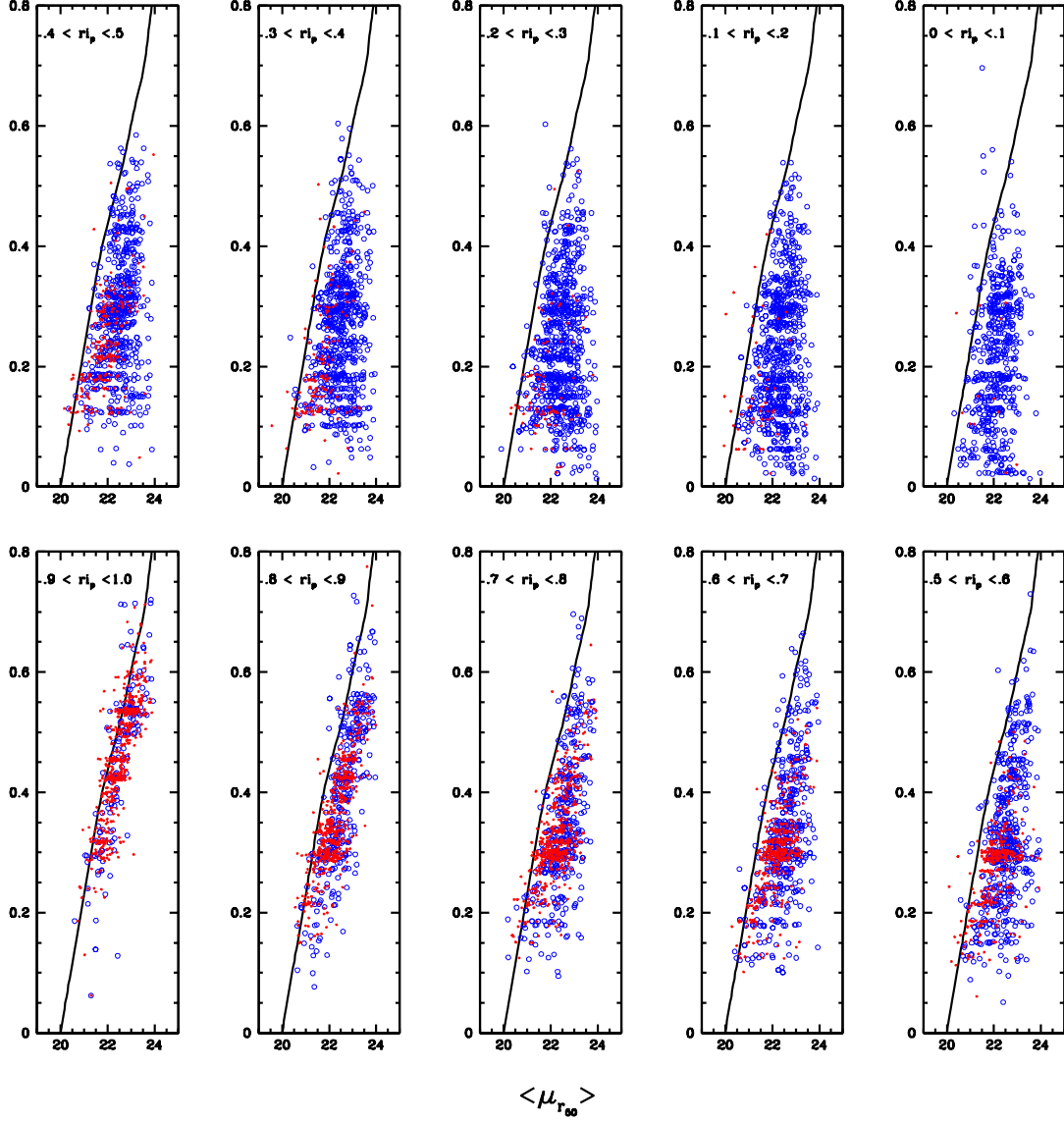


Fig. 3.— The redshift-surface brightness diagram for ten deciles in  $r$  surface brightness sorted ( $r - i$ ) color (Color Rank Percentile, see text). The (online blue) circles are objects with clear O[II] emission, the (red) dots are absorption line objects.

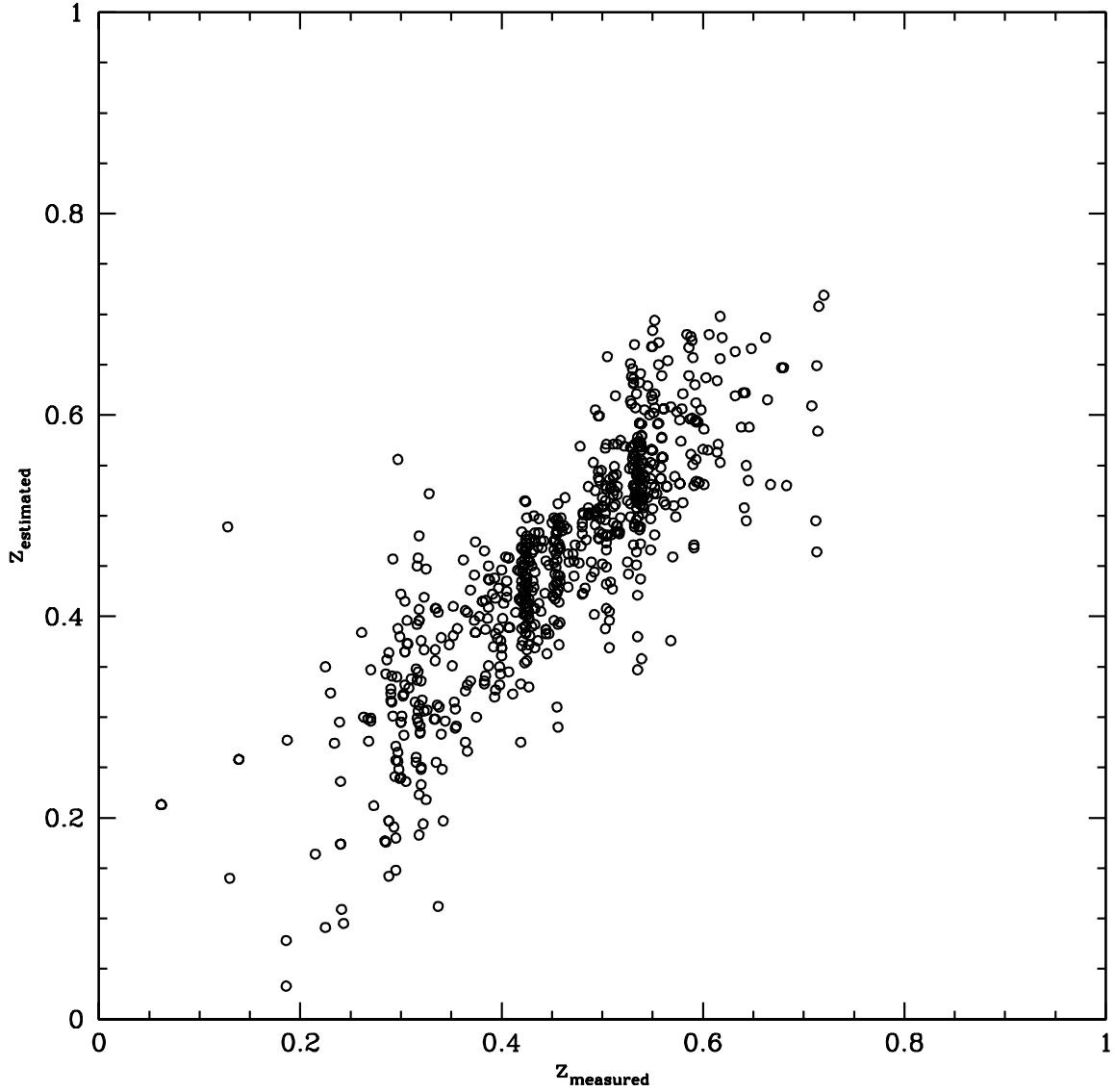


Fig. 4.— A comparison of the predicted and measured redshifts obtained by applying the model to the reddest 10% of galaxies.

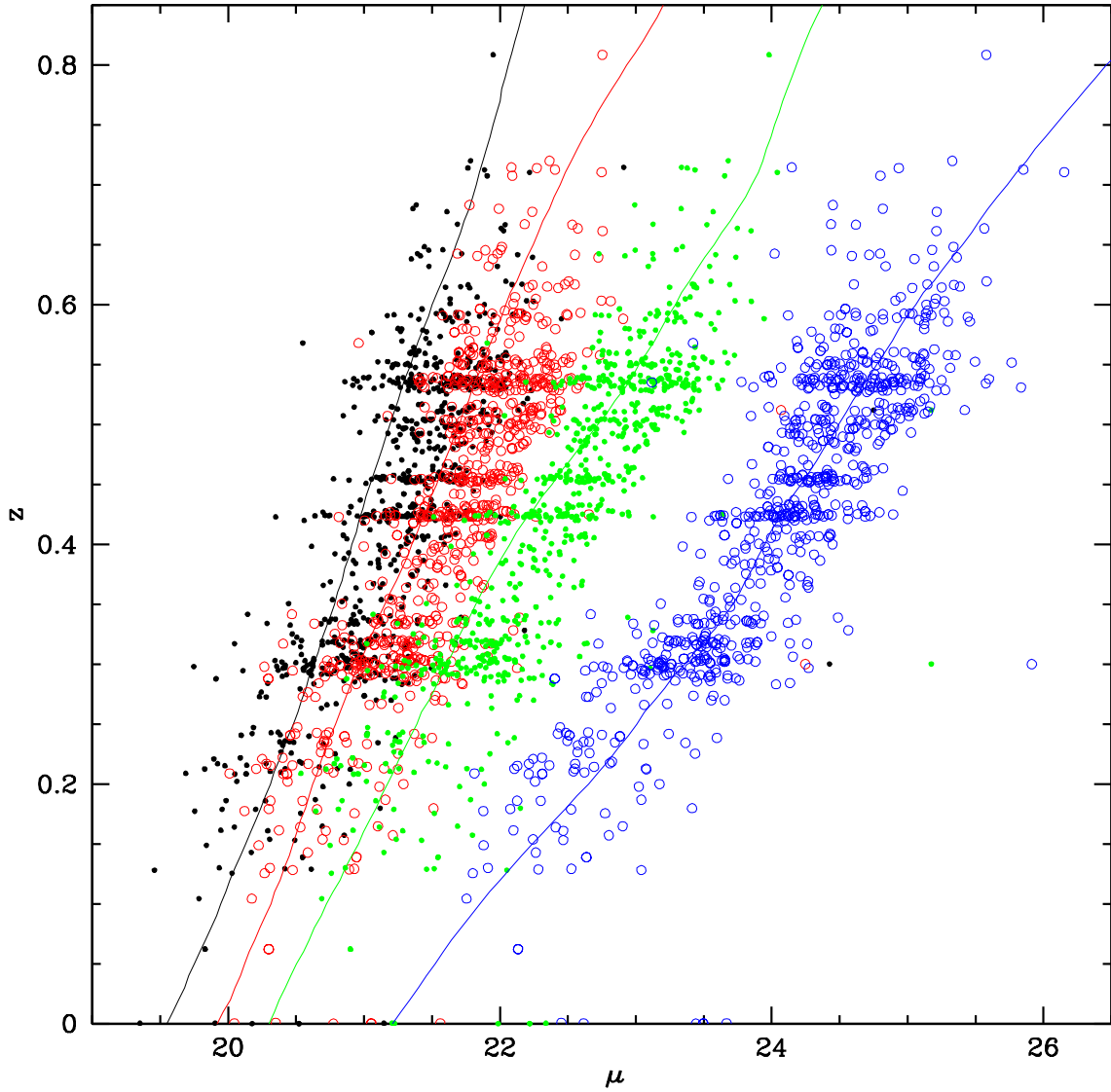


Fig. 5.— The surface brightness redshift relation for different color bands, for the reddest 10% in  $(r - i)$  selected at fixed  $\mu_r$ . The leftmost (black online) dots are the  $z$  band measure, the (red) circles are  $i$ , the (green) dots are  $r$ , and on the rightmost the (blue) circles are  $g$ . The lines are the Annis (2001) BCG K correction for the appropriate color.

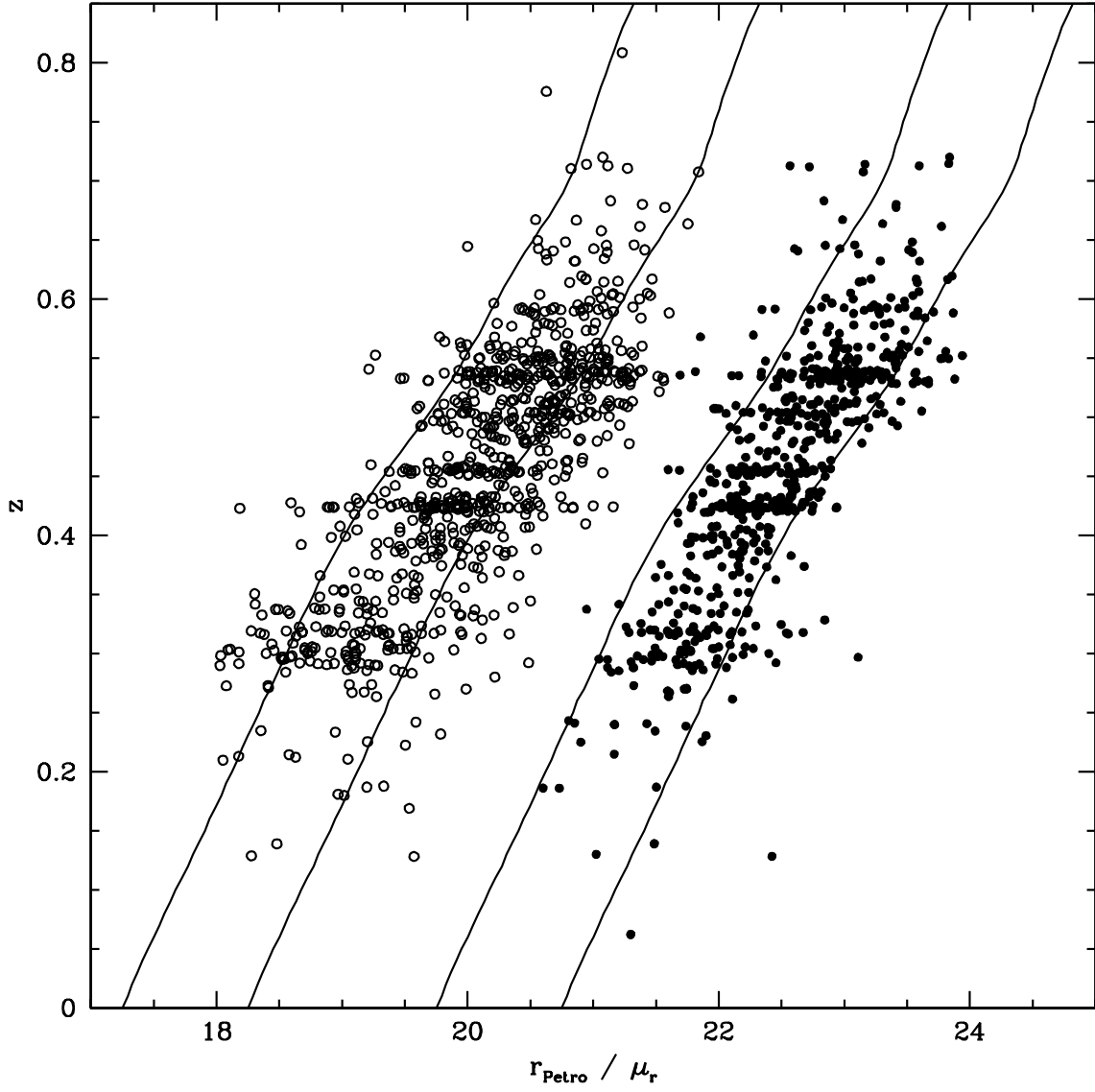


Fig. 6.— The difference between the reddest 10% using total Petrosian magnitudes (left) and  $\mu_r$  (right). Note the decreased scatter for  $\mu_r$ .

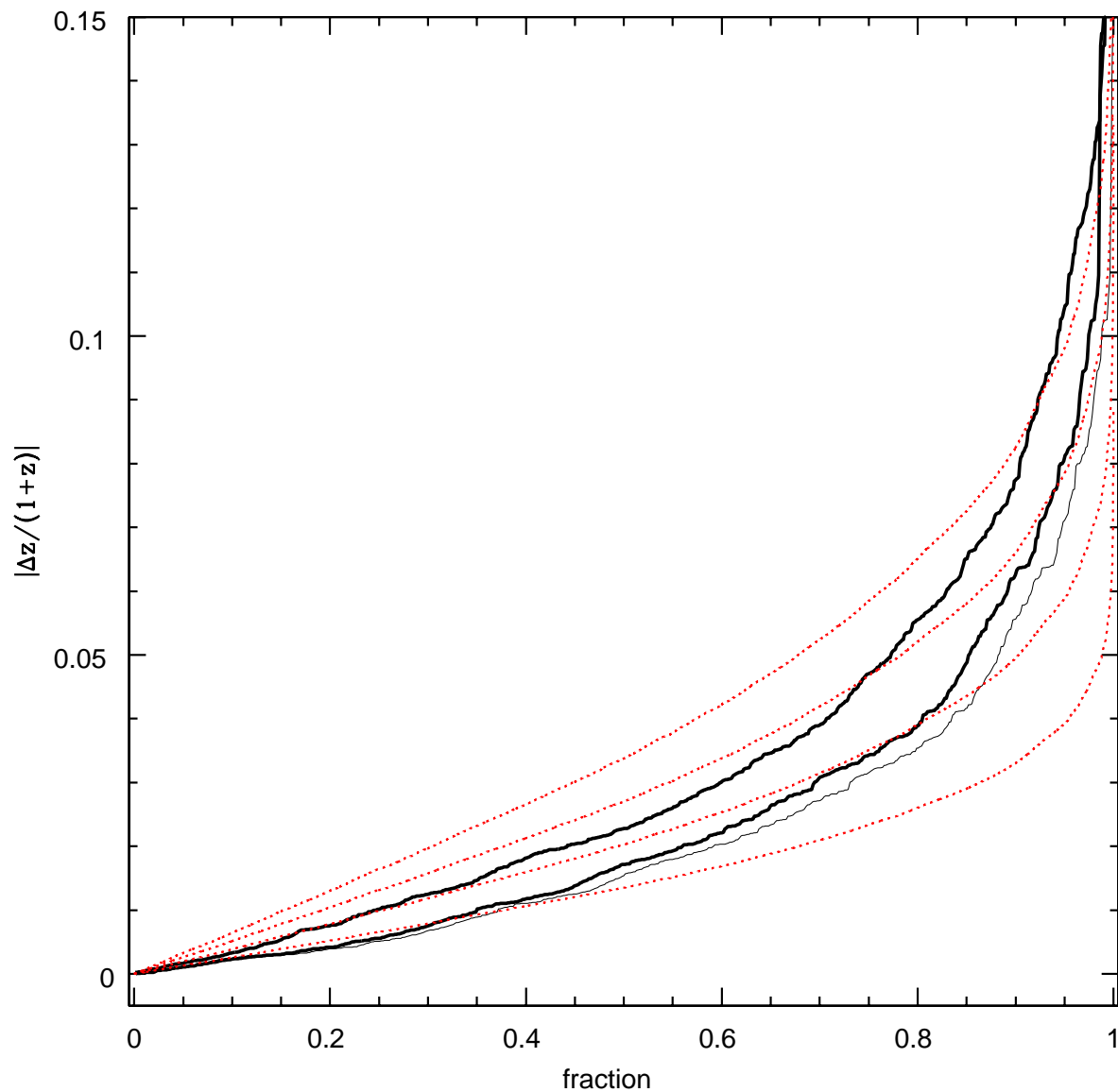


Fig. 7.— The sorted absolute value of the errors of the technique in section 5. The (red online) dotted lines represent normal error distributions, with  $\sigma$ s of 0.05 (top), 0.04, 0.03, and (bottom) 0.02. The thick lines represent the actual data for the reddest 80-90% (top) and the reddest 90-100% (bottom). The thin solid line and the lower solid thick line differ by the removal of all objects with  $(g - r) < 1.4$  for the thin line.

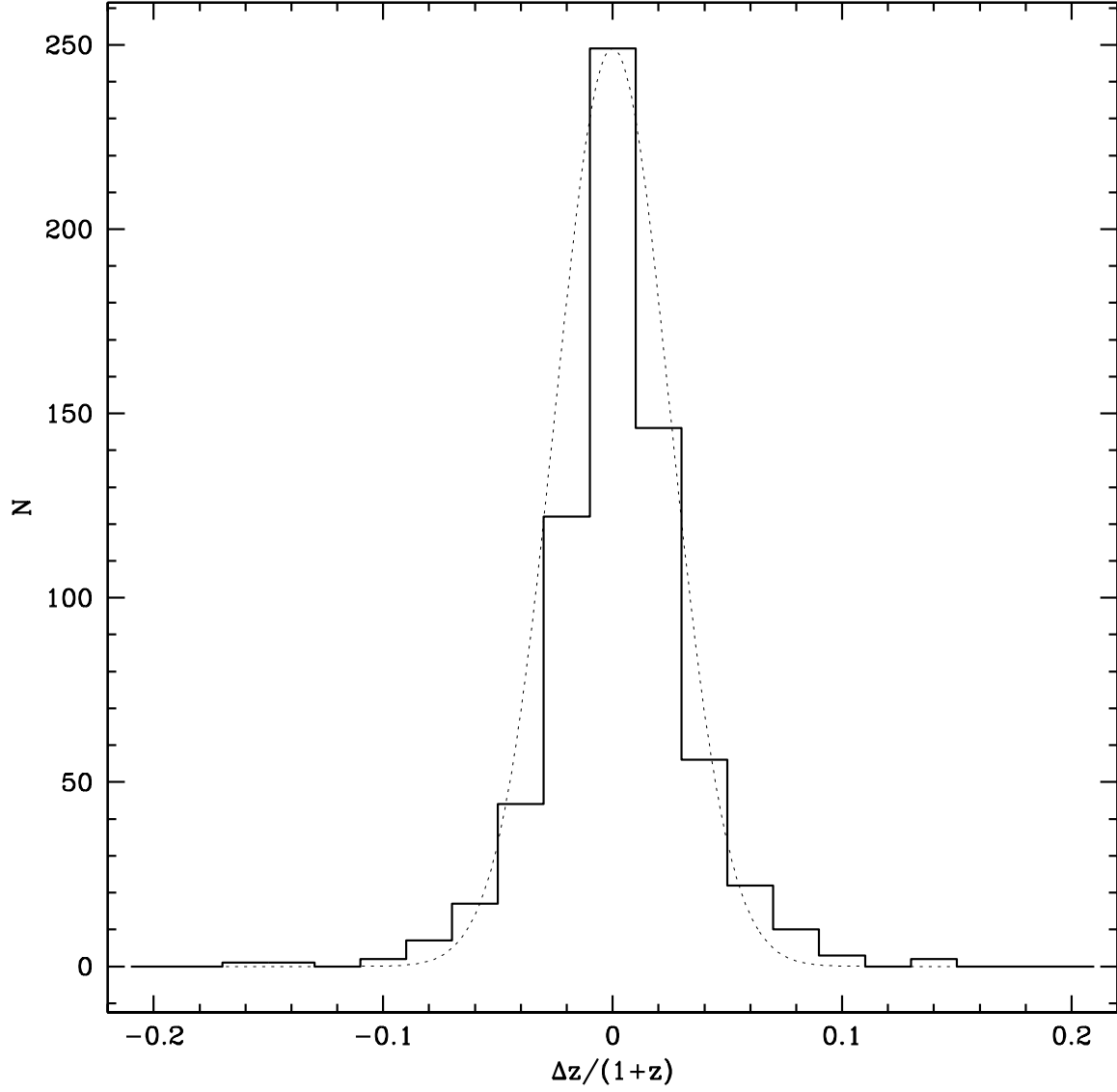


Fig. 8.— The error distribution ( $\frac{\Delta z}{1+z}$ ) for the 80-100% reddest objects, with the  $(g-r) < 1.4$  objects removed. The gaussian has  $\sigma = 0.025$ .

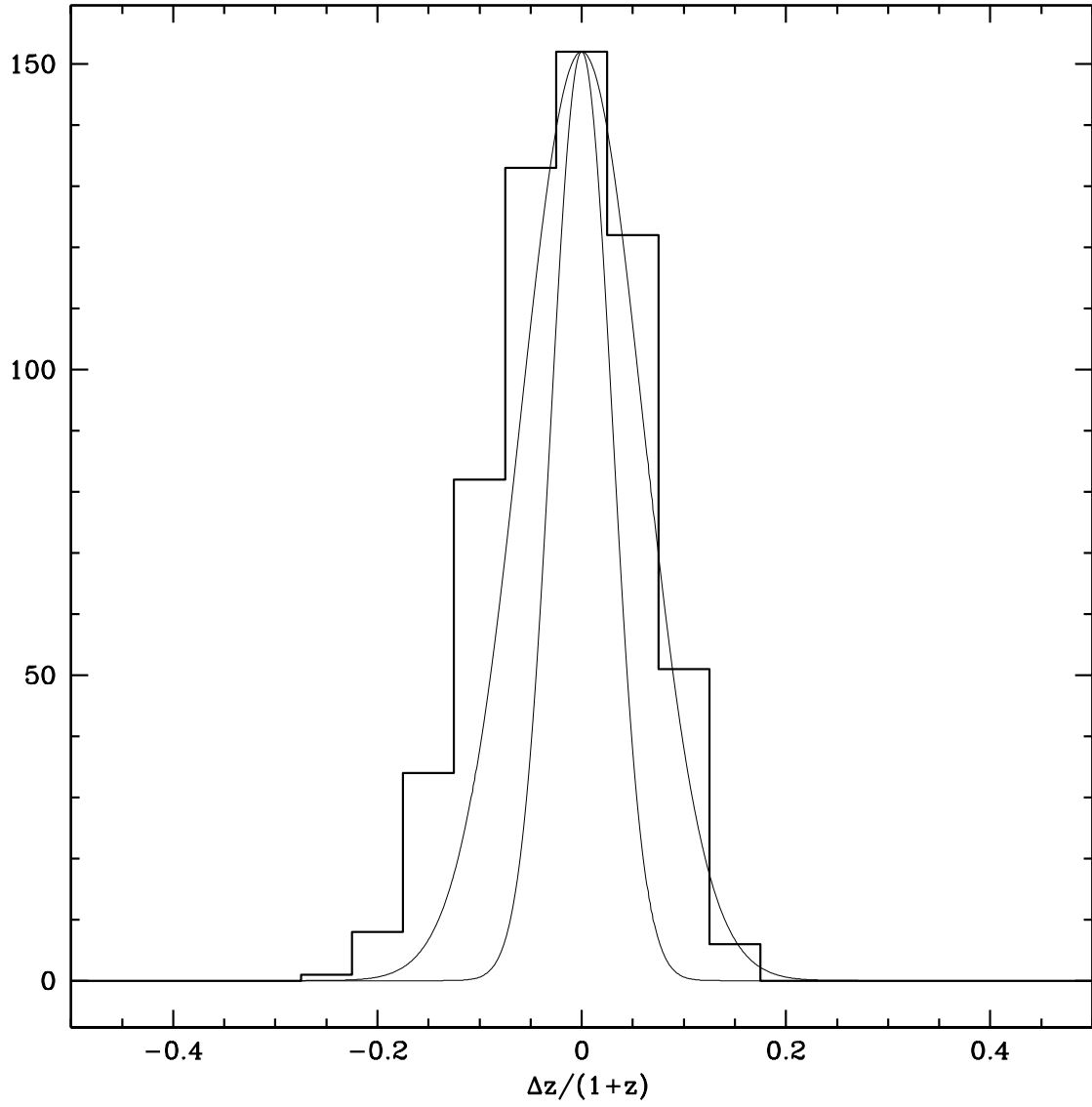


Fig. 9.— The error distribution ( $\frac{\Delta z}{1+z}$ ) for the 80-100% reddest objects, with  $(g - r) < 1.4$ . Gaussians with  $\sigma = 0.030$  and  $\sigma = 0.06$  are superposed. Note the change in scale from figure 8

Table 1. Redshift vs.  $\mu_r$  and  $(r - i)$

$\mu_r$	0.50	0.55	0.60	0.65	0.70	0.75	0.80	0.85	0.90	0.95	1.00	1.05	1.10	1.15	1.20
20.40															
20.50															
20.60	0.228	0.258													
20.70	<b>0.246</b>	0.255													
20.80	<b>0.235</b>	<b>0.265</b>													
20.90	<b>0.247</b>	<b>0.262</b>	0.289	0.336											
21.00	<b>0.247</b>	<b>0.268</b>	<i>0.297</i>	0.287											
21.10	<b>0.252</b>	<b>0.275</b>	0.295	0.316											
21.20	<b>0.258</b>	0.280	0.307	<i>0.312</i>	0.294										
21.30	0.262	0.282	0.314	0.329	0.331										
21.40	0.266	0.292	0.318	0.335	0.366										
21.50	0.271	0.296	0.322	0.345	<i>0.353</i>										
21.60	0.280	0.303	0.327	0.343	0.366	<i>0.391</i>									
21.70	0.295	0.313	0.335	0.353	0.370	<i>0.400</i>									
21.80	0.303	0.319	0.337	0.353	0.375	<i>0.409</i>	<i>0.422</i>	<i>0.421</i>							
21.90	0.305	0.320	0.342	0.361	0.382	0.414	0.432	<i>0.458</i>							
22.00	0.318	0.330	0.343	0.364	0.388	0.409	0.432	0.450	0.469	0.476					
22.10	0.319	0.334	0.351	0.371	0.396	0.419	0.440	0.455	0.466						
22.20	0.327	0.341	0.357	0.377	0.398	<b>0.421</b>	0.444	0.458	<b>0.466</b>	0.471	0.479				
22.30	0.337	0.346	0.363	0.382	0.404	0.425	<b>0.439</b>	0.452	<b>0.471</b>	0.475	0.488				
22.40	0.343	0.354	0.365	0.388	0.403	<b>0.427</b>	<b>0.444</b>	0.463	<b>0.471</b>	<i>0.480</i>	0.478				
22.50	0.352	0.361	0.374	0.391	0.410	0.429	<b>0.448</b>	<b>0.458</b>	0.473	<b>0.485</b>	<i>0.490</i>	0.505			
22.60	0.360	0.367	0.382	0.395	0.416	<b>0.435</b>	<b>0.450</b>	<b>0.463</b>	0.476	<i>0.489</i>	<i>0.496</i>				
22.70	0.364	<i>0.363</i>	0.381	0.402	0.420	<b>0.441</b>	<b>0.456</b>	<b>0.466</b>	<b>0.472</b>	<b>0.489</b>	<b>0.500</b>	<i>0.509</i>	0.509		
22.80	<i>0.380</i>	0.373	0.393	0.410	0.421	<b>0.445</b>	0.460	<b>0.468</b>	<b>0.481</b>	<i>0.485</i>	0.503		0.523		
22.90	<i>0.358</i>	0.386	0.403	0.415	0.429	0.451	<b>0.455</b>	<b>0.472</b>	<b>0.483</b>	<b>0.494</b>	0.504	<b>0.514</b>	0.524	0.535	
23.00	0.397	<i>0.388</i>	<i>0.405</i>	0.419	0.439	0.451	<b>0.464</b>	<b>0.478</b>	<b>0.484</b>		<b>0.505</b>	<b>0.523</b>	0.548		
23.10	<i>0.401</i>	0.398	0.413	0.429	0.445	0.458	<b>0.468</b>	<b>0.483</b>	<i>0.484</i>	<b>0.502</b>	<i>0.512</i>	0.528		0.515	
23.20		0.405	0.424	<i>0.429</i>	0.449	0.463	<i>0.474</i>	<i>0.488</i>	<b>0.489</b>	<b>0.509</b>	0.500		0.537	0.539	

Note. — The fonts indicate the measured errors in each cell, where  $\sigma_1$  is the estimate of  $\sigma_{\Delta z/(1+z)}$  obtained at the 68% point in the error distribution and  $\sigma_2$  is obtained at the 95% point. **Bold:**  $\sigma_1 < 0.025, \sigma_2 < 0.035$ ; Roman:  $\sigma_1 < 0.035, \sigma_2 < 0.05$ ; *Italic:*  $\sigma_1 < 0.05, \sigma_2 < 0.07$ ; Typewriter:  $\sigma_1 < 0.035, \sigma_2$  undefined (fewer than 30 objects in the bin).